Science of Sintering, **56** (2024) 89-103

https://doi.org/10.2298/SOS230701041H

UDK: 622.785; 661.112.3; 666.3.019

Influence of Sintering Temperature on Structure, Physical, and Optical Properties of Wollastonite based Glass-Ceramic Derived from Waste Eggshells and Waste Soda-Lime-Silica Glasses

Chen Hongxu[1], Raba'ah Syahidah Azis[2*)], Mohamad Hafiz Mohd Zaid[1,2], Khamirul Amin Matori[1,2], Ismayadi Ismail[2]

[1]Institute of Nano Science and Nano Technology, Universiti Putra Malaysia 43400 UPM Serdang, Selangor, Malaysia

[2]Department of Physics, Faculty of Science, University Putra Malaysia, 43400 UPM, Serdang, Selangor, Malaysia

Abstract:

Calcium oxide from discarded eggshells and waste soda-lime-silica were utilized in this study to make wollastonite ($CaSiO_3$) based glass-ceramics. The calcium oxide and silica were made using the melt-quenching process and sintered for 2 hours at 700 to 1000 °C. The XRD data verified that the wollastonite crystalline peak appeared at high sintering temperatures, with crystalline phase values of 39.74%, 47.37%, and 48.91% as the sintering temperature increased at 800-1000°C, respectively. Additionally, crystalline size and phase have no obvious change at 800-1000°C, where the intensity has increased by the sintering temperature. The FTIR spectra revealed the wollastonite phase vibration at the wavelength of 501, 650, 715, 808, 931, and 2129 cm^{-1}. Additionally, the FTIR spectral confirm the Si-O-Ca vibration band at the wavelength of 650 cm^{-1}. For the optical sample, the value of indirect allowed transition with n=2 is the ideal value of the optical band gap based on a band gap rise from 3.89 to 4.23 eV with increasing sintering temperature. The value n=2 which is the indirect allowed transition is the optimal value of the optical band gap based on the value increase from 3.89-4.23 eV as the temperature increase. The synthesis approach introduced the low-cost method, recycle approach, simple and yet uses cheap starting materials for fabrication of wollastonite glass-ceramics product.

Keywords*: Waste glass; Melt quenching; Density; XRD; UV-Vis.*

1. Introduction

Wollastonite is also known as calcium silicate ($CaSiO_3$) and is a calcium inosilicate found in nature [1]. Triclinic wollastonite, monoclinic wollastonite, and triclinic wollastonite are the three types of high-temperature wollastonite. The type of wollastonite used at high temperatures is cyclo-wollastonite [2]. Wollastonite is currently widely employed in ceramics fabrication, metallurgical processing, architecture, construction, glass glazes, and a variety of other industrial sectors [3]. Wollastonite was frequently employed in coat implants in earlier research to stimulate pulp regeneration, bone regeneration, and dental tissue remineralization. These important qualities include high bioactivity, excellent mechanical capabilities, and high porosity [4]. The structure of para-wollastonite is unusual, having lengthy chains of silicon tetrahedra $(SiO_4)_4$ [5].

*) **Corresponding author:** rabaah@upm.edu.my

Eggs were frequently used as foods and consumables as waste products. As a result, some articles suggested that recycled eggshells may be used as a new low-cost application material to safeguard the environment [6]. Egg-shell waste (ESW) is a type of agricultural waste that is typically regarded useless and abandoned, and it also contributes to environmental damage [7]. Calcium carbonate (96%), magnesium carbonate (1%), calcium phosphate (1%), and organic materials comprise up the chemical composition of eggshells (by weight) [8]. Eggshells can also be used as a source of $CaCO_3$ in various applications, such as limestone or lime [9]. The ESW can create hydroxylapatite, which is useful for bone repair and tissue regeneration [10], as well as bone and teeth. [11].

Soda-lime-silica formed by these substances, which contains 70% silica (SiO_2), 12-15% sodium oxide (Na_2O), 10%-15% calcium oxide (CaO), potassium oxide (K_2O), and aluminum oxide (Al_2O_3) [12], and soda-lime-silica (SLS) glass waste has a large volume globally [13]. SLS glass can recycle and synthesize new material based on benefits softened due to its softening [14] and remelted numerous times properties, excellent resistance to thermal shock strong thermal shock resistance, high UV transparency, non-electrical conductors, low melting point, good outstanding chemical stability and are diamagnetic characteristics diamagnetic properties [15,16]. Packaging, glass containers, windows, glass housing, insulating materials, and bioactive material industries are among the areas that use SLS glasses [17, 18]. Some earlier articles claim that reusing SLS glass to create glass-ceramic is a cost-effective and environmentally friendly solution to substitute silicon dioxide (SiO_2) resources [19]. Hou et al, Glass samples of $15CaO\text{-}65SiO_2$ were sintered at 800-1000°C for 2 hours to produce the only crystalline phase which is the wollastonite [20]. The crystallinity of wollastonite was found to be altered by autoclaving and sintering parameters in a recent study [21]. According to a previous study, α-wollastonite glass-ceramic is built of collaborative pseudo-wollastonite and amorphous phase at 1200 °C [22]. On the basis of Na-Ca-phosphate and fluorapatite, Mahdy et al. created a glass-ceramic base. They discovered that the density of samples with glass-ceramic was better than that of matching glass samples, with density values ranging from (2.50-2.92 g/cm^3). According to the article, density is created by increasing temperature during the heat treatment process, which causes the remaining pores to disappear or the creation of increasingly denser crystalline phases [23]. The volumetric density (2.82 g/cm^3) of glass-ceramics generated from tailings waste ($CaO\text{-}Al_2O_3\text{-}SiO_2$) at 950°C for 2 hours was reported in a previous article [24]. Although some articles have reported the production process of glass ceramics [25,26], it is still essential to focus on developing cost-effective and recyclable materials to enhance the production efficiency of glass ceramics. Additional data is necessary to explore the factors influencing the formation of wollastonite glass-ceramics with physical, structural, and optical properties, intending to reduce manufacturing costs and optimize the process of forming glass ceramics. As a result, the ESW and SLS waste glasses will be highlighted and are the main interest of this study due to their excellent mechanical and optical qualities and good chemical stability in producing wollastonite glass-ceramic [1]. Wollastonite glass-ceramic uses $CaO\text{-}SiO_2\text{-}B_2O_3$ as raw materials and is efficiently produced by melt quenching and sintering methods. This paper investigated the effect of sintering temperature on the formation of glass ceramics and provided more insights into the efficient glass-ceramic process with the optimum calcium oxide content.

2. Materials and Experimental Procedures

2.1. Preparation of Sample

As part of the preparation process for obtaining CaO powder and SLSW powder, the raw materials of soda-lime-silica glass (SiO_2) waste (SLSW) and eggshell ($CaCO_3$) waste (ESW) was cleaned and dried. The source glass bottles, the SLSW glass wastes were gathered

from the South City Plaza Serdang, Selangor, Malaysia. The eggshell debris was recovered from a restaurant in Putrajaya, Malaysia. The eggshells were processed CaO by heating temperature is 900°C for 2 hours and the sieving size of a particle is 45 μm. SLSW powder with a particle size of 45 μm was prepared by crushing, plunging, milling and sieving. An electronic digital balance was used to weigh both the ES and SLS powders with an accuracy of 0.0001g. Table I and Table II show a group of preparation samples that empirical formula is $[ESW]_x[SLSW]_{100-x-15}$ $[B_2O_3]_{15}$ where x= 5 wt.%, 10 wt.%, 15 wt.% with 40g as total weight via melt-quenching method at 1450°C with 3 hours 15 minutes. After melt-quenching, the homogenous glass powder was milled and sieved with a particle size of 45 μm. Using the Specac Manual Hydraulic Press and polyvinyl alcohol to produce a 13mm-diameter and 2mm-thickness pellet. To produce crystallization, place the pellet-sinter in the air for 2 hours at varying temperatures (700°C-1000°C) at a slow heating rate of 10 ℃/min. The sample preparation flow chart is shown in Fig. 1.

Tab. I Ratio of ESW to SLS glass powder with B_2O_3.

ESW (CaO)	SLSW	B_2O_3
5%	80%	15%
10%	75%	15%
15%	70%	15%

Tab. II The empirical formula and weight ratio of ESW (CaO) to SLSW glass.

Sample	Empirical Formula $[ES]_x[SLS]_{100-x-15}$ $[B_2O_3]_{15}$	Weight (g)		
		SLSW	B_2O_3	ESW(CaO)
1	5(ESW)80(SLSW)15(B_2O_3)	32	2	6
2	10(ESW)75(SLSW)15(B_2O_3)	30	4	6
3	15(ESW)70(SLSW)15(B_2O_3)	28	4	6

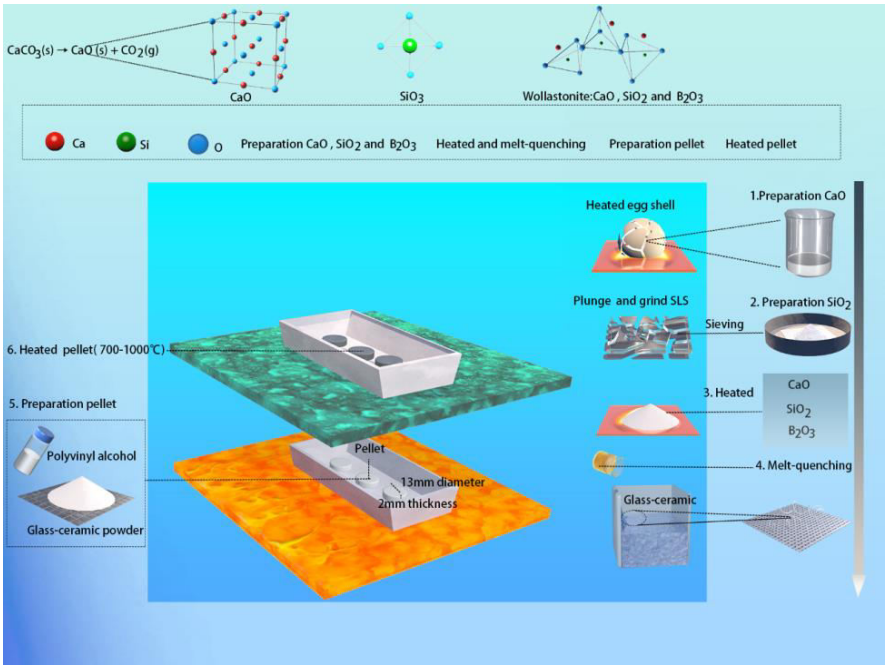

Fig. 1. Schematic of sample preparation.

2.2. Sample characterization

The XRD measurement analyzed the crystalline phase by utilizing PANalytical (Philips) X'Pert Pro PW3050/6 with Ni-filtered Cu-Ka radiation of 1.5406 Å, including the accelerating voltage 40 of kV and the input current of 40mA. The Fourier transforms infrared spectroscopy (FTIR) was conducted in the wave number range of 400-4000 cm^{-1}. The optical results of samples were evaluated using UV-Vis spectroscopy (UV-3600 UV-VIS-NIR), the transmission range of UV-Vis is between 220-2600 nm.

The bulk density ($\rho\ bulk$) of the samples was measured at room temperature, by Archimedes' principle with the formula as shown in Equation (1).

$$\rho_{bulk} = \left(\frac{W_{air}}{W_{air}-W_{water}}\right) \times \rho_{water} \qquad (1)$$

where W_{air} is a sample's weight in the air, W_{water} is a sample's weight in water and is a density of water (1 g/cm^3).

The sample's shrinkage (S) was determined as the percentage of length reduced in samples after heat treatment. The percent of the sample's shrinkage is calculated as in Equation (2):

$$LE = \frac{d_f - d_i}{d_i} \times 100\% \qquad (2)$$

where d_i is the pallet's diameter before sintering and d_f is the pallet's diameter after the sintering procedure. The linear expansion (LE) of the samples was measured by subtracting the sample's diameter (d_f) after sinter, which after the sinter sample's diameter to the diameter of the sample before sinter, initial diameter (d_i) using a digital vernier caliper (Mitutoyo 500-196-20, Kanagawa, Japan).

3. Results and Discussion

3.1. Physics Analysis

The density of glass-ceramics grew from 2.61 g/cm^3 to 2.83 g/cm^3 while sintering at 700-1000ºC, as shown in Fig. 2. Fig. 2 depicts the density increase with a constituent from the initiation density to reveal that the glass-ceramic formed base on the densification proceed in the based glass structure. Respectively, glass-ceramic whose CaO content is 15% at 1000°C was demonstrated that showed more efficient wollastonite to compare the rest of the sample by the theoretical density of wollastonite is 2.9 g/cm^3 [27]. Wollastonite has the largest bulk density (2.83 g/cm^3) when heated to 1000ºC, hence the density of the fabricated wollastonite glass-ceramic sample is around 97.5 percent of the theoretical density. This helps to explain why the sintering of the wollastonite sample was so effective. As a result, the density obtained using the Archimedes approach was shown to be extremely accurate in comparison to the theoretical value.

With a sintering temperature of 1000°C, the sample density was enhanced from 2.61 g/cm^3 to 2.83 g/cm^3, with a 5wt% to 15wt% content of ESW. The amount of crystallite has been increased where by sintering samples with high content of ESW CaO because the content of ESW CaO would affect the value of density [28]. Whereas the sintering temperature is another factor that affects the value of the wollastonite density. Fig. 2 indicated that the density of 5%-15% ES is increased by the temperature of 700°C up to 1000°C. The density of glass-ceramic increased with the sintering temperature because the glass-ceramic structure has densification and sedimentation of crystal. Densification of the sample occurs as

the pressure increases with the temperature increase, and the pores at high temperatures cause the sample to be denser [29].

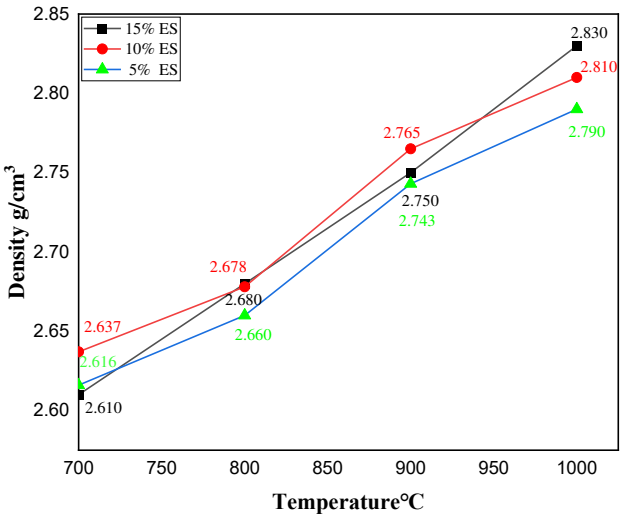

Fig. 2. Graph of density against temperature for different composition.

Tab. III Table of density and linear shrinkage against temperature for different composition.

Sample	Temperature (°C)	Density (g/cm^3)	Linear Shrinkage (%)
1	700	2.610	9.230
	800	2.680	9.760
	900	2.750	10.300
	1000	2.830	13.800
2	700	2.637	10.100
	800	2.678	12.760
	900	2.765	13.300
	1000	2.810	14.070
3	700	2.637	10.100
	800	2.678	12.760
	900	2.765	13.300
	1000	2.810	14.070
4	700	2.616	11.070
	800	2.660	13.300
	900	2.743	14.100
	1000	2.790	14.300

The linear shrinkage of the glass-ceramic samples with 15% ESW(CaO) against heat treatment temperature is shown in Fig. 3. The highest shrinkage percentage is 14.3% with 15%ESW by the sintering temperature increasing to the 1000°C and the lowest linear shrinkage of glass-ceramic is 9.23% with 5% ES when the sintering temperature is 700°C. Fig. 3 shows that the linear shrinkage increased as the sintering temperature rose, demonstrating that the kinetic energy of the material particles increased as the temperature rose, causing the particle to vibrate with high amplitude and causing particle diffusion. The size of the grains increases as the temperature increases while the porosity reduces [30]. The

sample forms a denser packing to cause the linear shrinkage to increase. This also indicates the efficiency of the sintering process. As introducing the temperature to the glass-ceramic samples, the bonding between particles is formed, mainly contributed by a diffusion process and accomplished by a decrease in volume, the shrinkage takes place and impairs the dimension and geometrical shape of the samples [31].

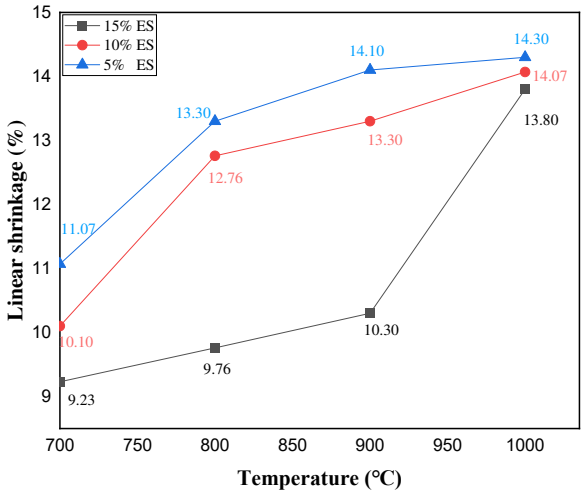

Fig. 3. Relationship of linear shrinkage against temperature for a different composition.

3.2. Structure Analysis

The XRD pattern of glass-ceramics after 2 hours of sintering at 70-1000°C is shown in Fig. 4. The XRD pattern revealed the phase of glass-ceramics lack of crystallization at 700°C by an amorphous hump at around the 2θ of 20° to 80°, whereas the wollastonite and quartz grew at the peak at 2θ = 27.84° when the temperature went up to 800°C. Some wollastonite-2M phase with ICSD reference code 76-1846 present with some amounts of anorthite ($CaAl_2Si_2O_8$) and small quantities of Quartz (SiO_2) as the temperature to 900°C and 1000°C. Respectively, the crystalline peak of quartz ($CaSi_2$) and peaks of wollastonite were exhibited in the XRD spectrum at 900°C and 1000°C to demonstrate the reaction between SiO_2 and CaO. The high sintering temperature would promote wollastonite growth in the pellet because more energy was supplied for rection, which interaction between CaO-SiO_2 to happen [32]. The amounts of wollastonite ($CaSiO_3$) were formed by increasing temperature by 900°C at these peaks, which are 2θ of 25.935°, 26.644°, 28.148°, 31.792°, 42.418°, 49.904°, and 51.838°. The crystallinity and crystal content (%) was determined using Equation (3):

$$C = \frac{A_C}{A_A + A_C} x100\% \qquad (3)$$

where C evaluates the crystallinity or the crystal content (%), Ac is the crystalline phase's diffraction peak area calculated using full width at half maximum (FHWM), and AA is the amorphous phase's scattering peak area. The optimum of wollastonite crystallinity is 48.91% where the heat treatment temperature at 1000°C compared with the wollastonite crystallinity is 47.37% and 39.74% at 800°C to 900°C, and the primary diffraction of optimum wollastonite peak at 25.743°, 26.516°, 27.575°, 28.011°, 28.546°, 31.565°, 43.355°, 49.765°, 50.805° and 51.65° to correspond the phase which is (3 1 1), (4 1 0), (0 2 1), (1 1 -2), (1 2 1),

(2 1 2), (6 1 -2), (3 2 3). The medium crystallite size (d) is evaluated whereby the Scherrer's equation formula:

$$d = \frac{0.9}{\beta} cos\theta \qquad (4)$$

where the equation is determined by the FHWM and depends on the peak position (2theta). The medium crystal size of wollastonite with a diffraction peak (1 1 -2) is 28.145 nm. The crystallite size results were tabulated in Table V to reveal no noticeable changes, which value is about 28 nm at 28.01°, 28.148°, and 28.048° peak positions with various temperatures. The intensity and quantity of wollastonite peaks will certainly grow as the sintering temperature rises to 900°C. The formation of wollastonite peak intensity is more robust by increasing the sintering temperature above 800°C through reactive crystallization. The formation of the primary crystalline phase was not affected, but it is also consistent with the increase in crystallinity and intensity of the sintered sample at temperatures above 1000°C [33].

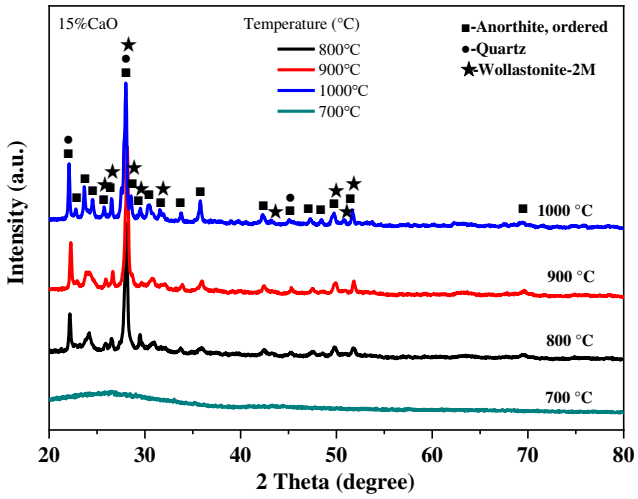

Fig. 4. XRD pattern of glass-ceramics with 15%CaO sintered at various temperature.

Tab. IV Crystalline size and Crystalline of glass-ceramic with 15% ES at various temperature.

Heat treatment T (ºC)	Peak position (2θ) (deg)	FWHIM (dθ)	Crystalline Size (nm)	Crystallinity (%)
700	—	—	—	—
800	27.800	0.344	27.770	39.740
900	28.148	0.345	27.940	47.370
1000	28.011	0.353	28.145	48.910

The FTIR spectra of 15%CaO sintered at 700°C to 1000°C with wave numbers 400 cm^{-1} to 4000 cm^{-1} are shown in Fig. 5. The IR absorption was analyzed with the previous study reference band as shown in Table V. The low frequency at 400-600 cm^{-1} demonstrates to exhibit of the Ca-O stretching and bending mode of O-Si-O [34, 35]. Fig. 4 depicts the Ca-O low-frequency band with 500 cm^{-1} to appear the glass-ceramic with 15% ES at 800-1000°C, inversely the FTIR spectra of glass-ceramic have no peak of Ca-O band by sintering temperature increase to 700°C. Respectively, the band of Ca-O was visible at a temperature of 800°Cdue to the wollastonite crystal phase being exhibited at high sintering temperature and

calcium oxide starting to saturate at 800°C [36]. The mid-frequency at 600-650 cm^{-1} can be referred to Ca-O-Si vibration band. The band at 650 cm^{-1} represents the Ca-Si-O band with a wide peak at 700°C, whereas the band appeared strong intense, and sharp peak with a sintering temperature increase of 800°C to demonstrate the formation of wollastonite by high sintering temperature and intense of wollastonite by increasing sintering temperature [37]. The two bands which the sintering temperature at 700-1000°C respective peak at 715 cm^{-1} and 812cm^{-1} were determined symmetric stretching vibration of Si-O and Si-O-Si bond bending by definition of the mid-band with wave numbers range from 600 cm^{-1} to 800 cm^{-1}. The frequency at 931 cm^{-1} and 1203 cm^{-1} relate to asymmetric stretching of Si-O and symmetric stretching of Si-O-Si bond [38, 39]. In fact, the Si-O band where the range of wave numbers located in 800-1250 cm^{-1} indicated an intense peak owing to the existence of silica in SLS glass powder [40]. The slight peak which was about 2050-2250 cm^{-1} indicated the ambient carbon dioxide and CO_2 in this glass-ceramic [15]. The modest peak rise in the 2050-2250 cm^{-1} range indicated the presence of carbon dioxide and CO_2 in glass-ceramic.

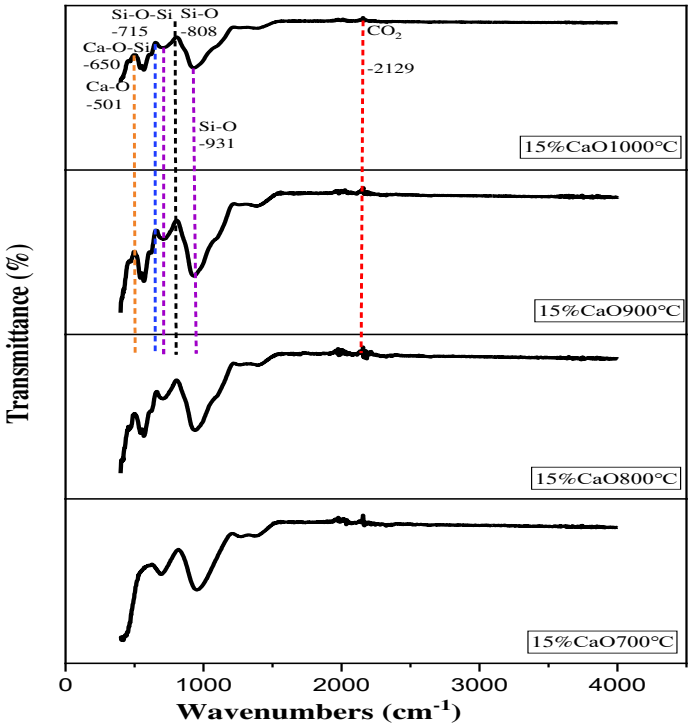

Fig. 5. FTIR spectra of glass-ceramic sintered at various temperatures.

Tab. V IR absorption of glass-ceramic with 15% ES sintered at various temperatures.

Wavenumber (cm^{-1})	Vibration Mode Assignment
400-600	Ca-O stretching mode, O-Si-O bending mode
600-650	Ca-O-Si vibration band
800-1250	Si-O symmetric stretching mode, O-Si-O bending mode

3.3. Optical Analysis

Tauc proposed utilizing optical absorption spectra to estimate the band gap energy of amorphous semiconductors in 1966. This study also uses the Tauc method to analyze the optical properties. The x-axis intersection point of the Tauc plot's linear fit approximates the

band gap energy [41]. The Tau technique is predicated on the idea that the energy -dependnt absorption coefficient may be state using the equation (6) below:

$$(\alpha h\nu)^{1/n} = C\,(h\nu - E_{opt}) \qquad (6)$$

which represents the optical absorption coefficient, α is the coefficient of absorption, h is Planck's constant, v is vibration frequency, C represents the constant independent of photon energy, and E_{opt} is the bandgap energy. The E_{opt} is determined by extrapolating the linear $(\alpha h\nu)^{1/n}$ versus $h\nu$ curves to $(\alpha h\nu)^{1/n} = 0$, n = 1/2 for direct allowed band gap transitions and $n = 2$ for indirectly allowed bandgap transitions [42]. UV-vis spectra of wollastonite glass-ceramic samples with 15% CaO at various sintering temperatures were observed in the 250-800 nm range. From a table of wollastonite glass-ceramic with 15% CaO in the 200-800 nm wavelength region, the energy bandgap was increased from 3.53 to 3.70 eV. The value of Eg corresponded to the direct allowed transition from 3.2 to 3.45eV, and the indirect allowed transition from 3.89 to 4.23eV given in the table to show the increasing of samples with progressing sintering temperature in Tab. VI. In the optical band gap value, the indirect allowed transition with n=2 is preferred over the E_{opt} (experimental) and direct allowed transition. Fig. 6 depicts intensive absorption; the absorption curve of wollastonite glass-ceramic increased with the sintering temperature increasing because of the indirect transition. Respectively, the energy band gap is more structural rearrangements depending on a scattering of short wavelength decrease with the increase of sizes and number of developed crystals as heat treatment duration progresses [43].

The UV-visible spectra of wollastonite glass-ceramic samples containing 15% CaO at different sintering temperatures were observed in the 250–800 nm range. As shown in Fig. 7, the value of Eopt (experimental band gap energy) gradually increases from 3.53 eV to 3.70 eV as the heat treatment temperature rises from 700°C to 1000°C. This indicates that the band gap energy of wollastonite glass ceramics increases with the heat treatment temperature. This may be due to the crystal structure rearrangement and defect density change due to heat treatment. As the size and number of crystals increase, the scattering at short wavelengths decreases, which may increase the energy band gap [33]. Secondly, we see a similar trend for the directly allowed transitions(n = 1/2), as shown in Fig. 8. The bandgap energy for the directly allowed leaps is 3.20 eV at 700°C, increasing to 3.45 eV at 1000°C. This further supports the idea that the thermal treatment increases the energy bandgap [33]. For indirectly allowed transitions (n=2), the increase in band gap energy is more significant from 3.89 eV to 4.23 eV, as shown in Fig. 9.

Tab. VI Optical band gap of the glass-ceramic with 15% CaO at various temperature.

Heat treatment (°C)	**E_{opt} (experimental) (eV)**	**Direct allowed transition n=1/2(eV)**	**Indirect allowed transition n=2(eV)**
700	3.53	3.20	3.89
800	3.57	3.25	3.96
900	3.64	3.37	4.05
1000	3.70	3.45	4.23

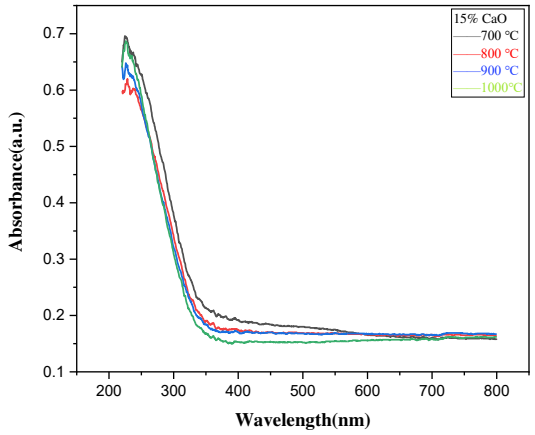

Fig. 6. Absorbance spectra of the glass-ceramic with 15% ES heated at various temperatures.

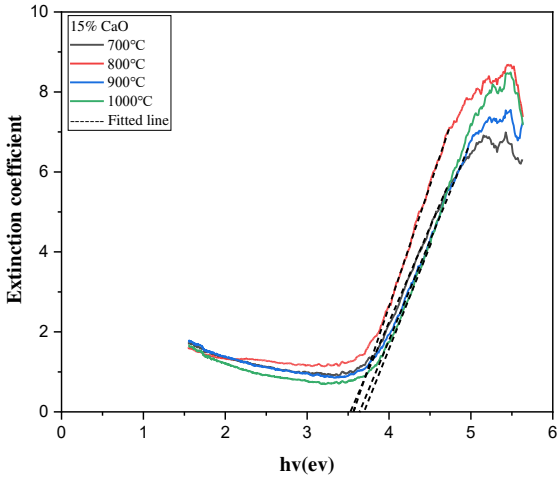

Fig. 7. Extinction coefficient against hv of glass-ceramic with 15% ES heated at various temperatures.

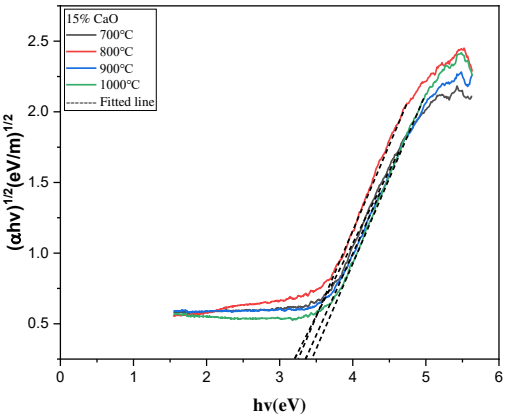

Fig. 8. The Direct allowed transition Tauc plots of glass-ceramic with 15% ES heated at various temperature.

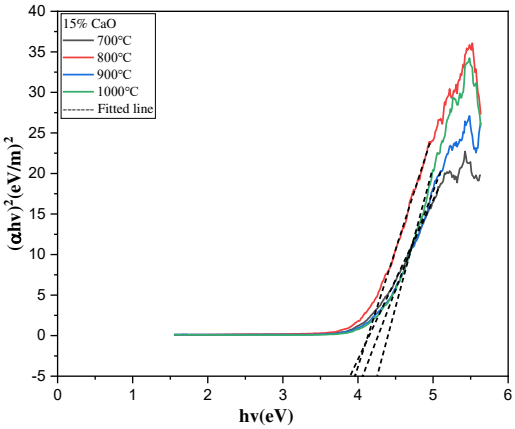

Fig. 9. The Indirect allowed transition Tauc plots of glass-ceramic with 15% ES heated at various temperatures.

4. Conclusion

Wollastonite glass-ceramic was effectively produced from SLS-CaO-B_2O_3 and made using melt-quenching and sintering methods. The sintering temperature influences the physics, structure, and optical properties of glass ceramics. The value of density and linear shrinkage rose as the sintering temperature was raised, due to the porosity reducing and forming a dense packing. The XRD results confirmed the wollastonite crystalline peak appeared at the high sintering temperature. The crystalline size and phase have no noticeable change at 800-1000°C, where the intensity has increased by the sintering temperature. The FTIR results confirm the CaO, SiO_2, and Ca-O-Si bands, showing the $CaSiO_3$ crystal formation at the wavelength of 650 cm^{-1}. The scattering of light with a short wavelength via the wollastonite crystals increased the optical band value as the sintering temperature increased, according to UV-vis measurements, highlighting the effect of sintering temperature on the optical properties of glass-ceramics. Overall, this study significantly advances our understanding of the interplay between sintering temperature and wollastonite glass ceramics' physical, structural, and optical properties. The research sheds light on these interactions, providing helpful information for optimizing the product act ion process and improving the overall qualities of glass-ceramic materials.

Acknowledgments

The authors acknowledge the Department of Physics, Faculty of Science, and the Institute of Nanoscience and Nanotechnology (ION2), Universiti Putra Malaysia, for providing the measurement facilities. The highest appreciation is given to the Universiti Putra Malaysia for the fund, grant No. GP-IPS/2021/9707200.

5. References

1. G.M. Azarov, E.V. Maiorova, M.A. Oborina, A.V. Belyakov. Glass and Ceramics. 52 (1995) 237-240.

2. S.R. Teixeira, A.E. Souza, C.L. Carvalho, V.C.S. Reynoso, M. Romero, J.M. Rincón, “Characterization of a wollastonite glass-ceramic material prepared using sugar cane bagasse ash (SCBA) as one of the raw materials,” Materials Characterization. 98 (2014) 209-214.
3. M.M. Mikhailov, S.A. Yuryev, A.N. Lapin, E.Y. Koroleva, V.A. Goronchko, “Optical properties degradation of wollastonite powders under the electron irradiation in vacuum,” Optical Materials. 119 (2014) 111-342.
4. S. Kunjalukkal Padmanabhan, F. Gervaso, M. Carrozzo, F. Scalera, A. Sannino, A. Licciulli, “ Wollastonite/hydroxyapatite scaffolds with improved mechanical, bioactive and biodegradable properties for bone tissue engineering”, Ceramics International. 39 (2013) 619-627.
5. L.Z. Zhu, H.Y. Sohn, T.M. Bronson, “Flux growth of 2M-wollastonite crystals for the preparation of high aspect ratio particles”, Ceramics International. 40 (2014) 5973-5982.
6. M. Mesri, Z. Shamsudin, R. Hasan, N. Daud “Effects of Bentonite and Eggshell as Fillers on Thermal Physical Properties of Sintered Glass Composite”, Journal of Advanced Research in Fluid Mechanics and Thermal Sciences. 66 (2020) 145-157.
7. R. Choudhary, S.K. Venkatraman, I. Bulygina, F. Senatov, S. Kaloshkin, N. Anisimova, M. Kiselevskiy, M. Knyazeva, D. Kukui, F. Walther, S. Swamiappan, “Biomineralization, dissolution and cellular studies of silicate bioceramics prepared from eggshell and rice husk”, Materials Science and Engineering: C. 118 (2021) 111456.
8. D.A. Oliveira, P. Benelli, E.R. Amante, “A literature review on adding value to solid residues: egg shells”, Journal of Cleaner Production. 46 (2013) 42-47.
9. D. Cree, A. Rutter, “Sustainable Bio-Inspired Limestone Eggshell Powder for Potential Industrialized Applications”, ACS Sustainable Chemistry & Engineering. 3 (2015) 941-949.
10. A.J. Salgado, O.P. Coutinho, R.L. Reis, “Bone Tissue Engineering: State of the Art and Future Trends”, Macromolecular Bioscience. 4 (2004) 743-765.
11. S. Ramesh, A.N. Natasha, C.Y. Tan, L.T. Bang, S. Ramesh, C.Y. Ching, H. Chandran, “Direct conversion of eggshell to hydroxyapatite ceramic by a sintering method”, Ceramics International. 42 (2016) 7824-7829.
12. J.H. Butler, P.D. Hooper, "Glass waste", in Waste: A Handbook for Management, 2nd ed.; T.M. Letcher, D.A. Vallero (eds), Academic Press: Cambridge, MA, USA (2019), pp. 307-322.
13. M. Z. A. Khiri, K. A. Matori, M. H. M. Zaid, A. C. Abdullah, N. Zainuddin, W. N. W. Jusoh, R. A. Jalil, N. A. A. Rahman, E. Kul, S. A. A. Wahab, and N. Effendy, "Soda lime silicate glass and clam Shell act as precursor in synthesize calcium fluoroaluminosilicate glass to fabricate glass ionomer cement with different ageing time", Journal of Materials Research and Technology. 9 (2020) 6125-6134.
14. V. Ducman, A. Mladenovič, and J. S. Šuput, "Lightweight aggregate based on waste glass and its alkali–silica reactivity", Cement and Concrete Research. 32 (2002) 223-226.
15. M. H. M. Zaid, K. A. Matori, L. C. Wah, H. A. A. Sidek, M. K. Halimah, and B. Z. Azmi, "Elastic moduli prediction and correlation in soda lime silicate glasses containing ZnO", International Journal of the Physical Sciences. 6 (2011) 1404-1410.
16. M. H. M. Zaid, K. A. Matori, H. A. A. Sidek, Z. A. Wahab, and S. S. A. Rashid, "Effect of sintering on crystallization and structural properties of soda lime silica glass", Science of Sintering. 49 (2017) 409-417.
17. J. M. Juoi, D. Arudra, Z. M. Rosli, K. Hussain, and A. J. Jaafar, "Microstructural properties of glass composite material made from incinerated scheduled waste slag

and soda lime silicate (SLS) waste glass", Journal of Non-Crystalline Solids. 367 (2013) 8-13.
18. J. M. Juoi, M. I. Ojovan, and W. E. Lee, "Microstructure and leaching durability of glass composite wasteforms for spent clinoptilolite immobilisation", Journal of Nuclear Materials. 372 (2008) 358-366.
19. V. W. Francis Thoo, N. Zainuddin, K. A. Matori, and S. A. Abdullah, "Studies on the Potential of Waste Soda Lime Silica Glass in Glass Ionomer Cement Production", Advances in Materials Science and Engineering. (2013) 1-6.
20. Y. Hou, G. H. Zhang, K. C. Chou, and D. Fan, "Effects of CaO/SiO2 ratio and heat treatment parameters on the crystallization behavior, microstructure and properties of SiO2-CaO-Al2O3-Na2O glass ceramics", Journal of Non-Crystalline Solids. 538 (2020) 120023.
21. H. Ismail, R. Shamsudin, M. A. Abdul Hamid, "Effect of autoclaving and sintering on the formation of β-wollastonite", Mater. Sci. Eng. C. 58 (2016) 1077-1081.
22. S. S. Hossain, S. Yadav, S. Majumdar, S. Krishnamurthy, R. Pyare, P. K. Roy, "Study of physical and dielectric properties of bio-waste-derived synthetic wollastonite", J. Asian Ceram. Soc. 6 (2018) 289-298.
23. E. A. Mahdy, H. Y. Ahmed, M. M. Farag, "Combination of Na-Ca-phosphate and fluorapatite in wollastonite-diopside glass-ceramic: degradation and biocompatibility", J. Non-Cryst. Solids. 566 (2021) 120888.
24. B. Li, Y. Guo, J. Fang, "Effect of crystallization temperature on glass-ceramics derived from tailings waste", J. Alloys Compd. 838 (2020) 155503.
25. F. He, Y. H. Zheng, & J.-H. Xie, “Preparation and properties of CaO-Al2O3-SiO2 glass-ceramics by sintered frits particle from mining wastes”, Science of Sintering. 46 (2014) 353–363.
26. N. Pallan, K. Matori, M. Hashim, R. Azis, N. Zainuddin, N. Pallan, F. Idris, I. Ibrahim, L. Wah, S. Rusly, N. Adnin, M. Khiri, Z. Alassan, N. Mohamed, & M. Zaid, “Effects of different sintering temperatures on thermal, physical, and morphological of SiO_2-Na_2O-CaO-P_2O_5 based glass-ceramic system from vitreous and ceramic wastes”, Science of Sintering. 51 (2019) 377–387.
27. I. H. M. Aly, L. Abed Alrahim Mohammed, S. Al-Meer, K. Elsaid, N. A. M. Barakat, "Preparation and characterization of wollastonite/titanium oxide nanofiber bioceramic composite as a future implant material", Ceram. Int. 42 (2016) 11525-11534.
28. D. I. Saparuddin, M. H. M. Zaid, H. A. A. Sidek, K. A. Matori, "Reuse of Eggshell Waste and Recycled Glass in the Fabrication Porous Glass–Ceramics", Appl. Sci. 10 (2020) 5404.
29. S. S. Hossain, P. K. Roy, "Study of physical and dielectric properties of bio-waste-derived synthetic wollastonite", J. Asian Ceram. Soc. 6 (2018) 289-298.
30. J. L. Amorós, E. Blasco, C. Feliu, A. Moreno, "Effect of particle size distribution on the evolution of porous, microstructural, and dimensional characteristics during sinter-crystallisation of a glass-ceramic glaze", J. Non-Cryst. Solids. 572 (2021) 121093.
31. W. N. W. Jusoh, K. A. Matori, M. H. M. Zaid, N. Zainuddin, M. Z. A. Khiri, N. A. A. Rahman, R. A. Jalil, E. Kul, "Effect of sintering temperature on physical and structural properties of Alumino-Silicate-Fluoride glass ceramics fabricated from clam shell and soda lime silicate glass", Results Phys. 12 (2019) 1909-1914.
32. S. Jaafar, M.H.M. Zaid, K.A. Matori, M.S.M. Ghazali, M. Shofri, N. Hisham, D. Saparudin, "Effect of sintering temperatures and foaming agent content to the physical and structural properties of wollastonite based foam glass-ceramics", Sci. Sintering. 52 (2020) 269-281.
33. K.A. Almasri, H.A.A. Sidek, K.A. Matori, M.H.M. Zaid, "Effect of sintering temperature on physical, structural and optical properties of wollastonite based glass-

ceramic derived from waste soda lime silica glasses", Results Phys. 7 (2017) 2242-2247.
34. A.M. Abdelghany, N.A. Ghoneim, H.A. ElBatal, "Characterization of Invert Soda Lime Silica Glasses Containing High Ti-tania Content Together with their Glass Ceramics", Silicon. 10 (2017) 1035-1043.
35. G. El Damrawi, R.M. Ramadan, M. El Baiomy, "Effect of SrO on the Structure of Apatite and Wollastonite Phases of Na2O-CaO-SiO2-P2O5 Glass System", New J. Glass Ceram. 11 (2021) 45-56.
36. D.I. Saparuddin, N.A.N. Hisham, H.A.A. Sidek, K.A. Matori, S. Honda, Y. Iwamoto, M.H.M. Zaid, "Effect of sintering temperature on the crystal growth, microstructure and mechanical strength of foam glass-ceramic from waste materials", J. Mater. Res. Technol. 9 (2020) 5640-5647.
37. N.A.N. Hisham, M.H.M. Zaid, H.A.A. Sidek, F.D. Muhammad, "Comparison of Foam Glass-Ceramics with Different Composition Derived from Ark Clamshell (ACS) and Soda Lime Silica (SLS) Glass Bottles Sintered at Various Temperatures", Materials. 14 (2021) 570.
38. V.S. Kumawat, A. Vyas, S. Bandyopadhyay-Ghosh, S.B. Ghosh, "Selectively modified nanostructured fluorcanasite glass-ceramic with enhanced micromechanical properties", J. Non-Cryst. Solids. 547 (2020) 120303.
39. A.P. Solonenko, A.I. Blesman, D.A. Polonyankin, "Preparation and in vitro apatite-forming ability of hydroxyapatite and β-wollastonite composite materials", Ceram. Int. 44 (2018) 17824-17834.
40. S.Y. Yao, P. Wang, D. Shao, H.X. Cao, W.W. Zhang, "Effect of ZnO on preparation and properties of CaSiO3 glass–ceramics", Mater. Res. Innovations. 18 (2014) S4-661S4-664.
41. P. Makuła, M. Pacia, W. Macyk, "How To Correctly Determine the Band Gap Energy of Modified Semiconductor Photocatalysts Based on UV–Vis Spectra", The Journal of Physical Chemistry Letters. *9*(2018) 6814–6817.
42. C.W. Mun, L.Z. Wei, M.H.M. Zaid, "The characteristics on structural and optical of Co3O4 incorporated Zn2SiO4 for phosphor approaches", J. Mol. Struct. 1248 (2022) 131474.
43. M.H.M. Zaid, H.A.A. Sidek, R. El-Mallawany, K.A. Almasri, K.A. Matori, "Synthesis and characterization of samarium doped calcium soda–lime–silicate glass derived wollastonite glass–ceramics", Journal of Materials Research and Technology, 9 (2020) 13153-13160.

Сажетак: *Калцијум оксид из одбачених љуски јајета и отпадни сода-креч-силицијум коришћени су у овој студији за прављење стаклокерамике на бази воластонита ($CaSiO_3$). Калцијум оксид и силицијум су направљени поступком топљења и синтеровани су 2 сата на 700 до 1000°C. XRD подаци су потврдили да се кристални пик воластонита појавио на високим температурама синтеровања, са вредностима кристалне фазе од 39,74%, 47,37% и 48,91% како се температура синтеровања повећала на 800-1000°C, респективно. Поред тога, величина и фаза кристала немају очигледне промене на 800-1000°C, где се интензитет повећава са температуром синтеровања. FTIR спектри су открили вибрације фазе воластонита на таласној дужини од 501, 650, 715, 808, 931 и 2129 cm^{-1}. Поред тога, FTIR спектар потврђује опсег вибрација Si-O-Ca на таласној дужини од 650 cm^{-1}. За оптички узорак, вредност индиректног дозвољеног прелаза са n=2 је идеална вредност оптичког појаса на основу пораста појаса од 3,89 до 4,23 eV са повећањем температуре синтеровања. Вредност n=2 која представља индиректни дозвољени прелаз је оптимална вредност оптичког појаса на основу повећања вредности од 3,89-4,23 eV са порастом температуре.*

Приступ овој синтези увео је ниске цене, приступ рециклажи, једноставан је, а користи јефтине почетне материјале за производњу воластонитне стаклокерамике.
***Кључне речи**: Отпадно стакло; топљење; густина; XRD; UV-Vis.*